Coherent optimal control of photosynthetic molecules

F. Caruso,[1,2] S. Montangero,[3] T. Calarco,[3] S. F. Huelga,[1] and M. B. Plenio[1]
[1]*Institut für Theoretische Physik, Universität Ulm, Albert-Einstein-Allee 11, D-89069 Ulm, Germany*
[2]*LENS and Dipartimento di Fisica e Astronomia, Università di Firenze, I-50019 Sesto Fiorentino, Italy*
[3]*Institut für Quanteninformationsverarbeitung, Universität Ulm, Albert-Einstein-Allee 11, D-89069 Ulm, Germany*
(Received 8 July 2011; revised manuscript received 11 April 2012; published 30 April 2012)

We demonstrate theoretically that open-loop quantum optimal control techniques can provide efficient tools for the verification of various quantum coherent transport mechanisms in natural and artificial light-harvesting complexes under realistic experimental conditions. To assess the feasibility of possible biocontrol experiments, we introduce the main settings and derive optimally shaped and robust laser pulses that allow for the faithful preparation of specified initial states (such as localized excitation or coherent superposition, i.e., propagating and nonpropagating states) of the photosystem and probe efficiently the subsequent dynamics. With these tools, different transport pathways can be discriminated, which should facilitate the elucidation of genuine quantum dynamical features of photosystems and therefore enhance our understanding of the role that coherent processes may play in actual biological complexes.

DOI: 10.1103/PhysRevA.85.042331 PACS number(s): 03.67.Ac, 03.65.Yz, 05.10.−a, 88.20.jr

I. INTRODUCTION

Recent experimental work has provided evidence supporting the existence of long-lived coherence during excitation energy transfer (EET) in photosynthetic complexes [1–5]. Subsequent theoretical work has then highlighted the importance of an intricate interplay of noise and quantum coherence for the remarkably high EET efficiency in light-harvesting complexes during photosynthesis and identified the crucial building blocks that underly this interplay [6–12]. While computer simulations and analytical work allow for the identification and direct verification of the importance of these effects in theory, the experimental verification of their relevance in actual biomolecular systems is still outstanding. One path toward achieving this goal is the application of optimal control methods that allow for the preparation of specific initial states of the system and control of the subsequent quantum dynamics in contact with its biomolecular environment. As a consequence, the dynamical behavior, and hence the resulting signals, can be made to exhibit the largest discrepancies between alternative hypotheses concerning properties of the dynamics of biomolecular systems. Implementing such optimal control methods would therefore allow us to develop strategies for gaining the maximal ability to obtain information about coherent processes in biological systems. Quantum coherent control drives the dynamics of a quantum system toward a specific goal by exploiting quantum coherence and interference effects [13]. Coherent control techniques have been proposed for photochemical and photobiological processes; see Refs. [14–16] for an overview of this topic. Evidence of control of exciton states in light-harvesting systems was presented in Ref. [17], based on genetic algorithms which, however, provide highly structured pulses, quite small signal-to-noise ratios, and only population control. An attempt to use open-loop optimization to control the exciton dynamics of a light-harvesting system was theoretically provided in Ref. [18], but the control algorithm employed there imposed some limitations to their analysis: complicated derivative functional equations, relatively long and highly complex pulses, large optimal relative errors (around 60% at 77 K for site-6 localization), and, again, only local state population. Here we will show that besides the ability to prepare superposition states on demand, we will obtain short, simple, and robust optimal pulses with relative errors always smaller than 20%, even in the presence of quite strong dephasing noise, by using a recently introduced versatile and efficient optimization algorithm (CRAB) [19]. The main goal of this work is to prepare the basic ground for a new generation of control experiments, demonstrating the feasibility of using coherent control to explore quantum properties of biological molecules. Moreover, this represents an application of CRAB to open many-body quantum systems. In particular, we apply quantum (open-loop) optimal control theory to the dynamics of the electronic excitations in the Fenna-Matthews-Olson (FMO) complex, which is a biological pigment-protein complex involved in the early steps of bacterial photosynthesis [2,3]. By using the CRAB approach in the context of the FMO complex, we (i) achieve general state preparation, thus allowing us to prepare specific initial states, especially fast and slow propagating states exhibiting constructive or destructive interference, by means of weak pump pulses; (ii) explore experimental constraints and imperfections (adapted to a realistic experimental setup); and (iii) optimize the difference in signals for different preparations to test theoretical hypotheses concerning complex dynamics. These tools provide an opportunity to verify competing microscopic EET models, since they yield distinct transport properties and, hence, respond differently to optimally shaped laser pulses, which are obtained in the context of a specific theoretical framework.

The paper is organized as follows. In Secs. II and III, we describe the background of optimal control theory and the theoretical model for the FMO complex, which we use as a specific application of our approach. Then, we discuss the target of our optimizations (Sec. IV), and the obtained results for single molecules and ensembles are shown in Secs. V and VI, respectively. The robustness of the optimal pulses, as well as when inhomogeneous broadening effects are included, is discussed in detail. The transfer efficiency features, related to our optimally prepared initial states, hence slow and fast transport pathways, are described in Sec. VII. Moreover, the presence of orientation disorder is exploited during the

optimization procedure in Sec. VIII, and for the probe pulse in Sec. X. Finally, it turns out that the achieved fidelities are even better when a partial orientation of the sample is performed (Sec. IX). The conclusion and final remarks are presented in Sec. XI.

II. OPTIMAL CONTROL: BACKGROUND AND METHOD

Protocols for coherent control of exciton states in light-harvesting systems were theoretically proposed in [18] and experimentally demonstrated in [17]. In Ref. [17], feedback-optimized femtosecond pulses are applied to the LH2 antenna complex from Rhodopseudomonas acidopila and to a bioinspired artificial dyad molecule in order to control the efficiency of the light-harvesting dynamics. Specifically, they optimize the branching ratio of energy transfer between intra- and intermolecular channels in the complex's donor-acceptor system and obtain an enhancement of about 30% in the LH2 system and about 10% in the artificial dyad molecule by shaping the pulses, employing feedback in an iterative learning loop scheme.

In all experimental demonstrations of control of photochemical and photobiological processes [14–17,20–22], closed-loop optimization by evolutionary algorithm was applied [23]. This procedure consists of three basic components: (1) a pulse shaper, generating the pulse shape to be tested; (2) the experiment, generating the feedback signal by pump-probe spectroscopy; and (3) a computer, running the learning algorithm and driving the optimization. Hence, the closed-loop optimization proceeds along the following steps: (i) a random guess of a set of pulses is shaped through the pulse shaper and then tested on the sample; (ii) the feedback signal is evaluated and used to start an evolutionary genetic algorithm (based on selection of "parents," "mutations," "recombination," and "generation" of new sets of pulse shapes); and (iii) a new set of pulses is obtained through the pulse shaper and applied to the sample. These steps will be repeated until the optimization has converged by following the so-called learning curve. Despite the interesting applications of this technique, closed-loop optimization tends to be effective only for population control, while coherent control experiments cannot be performed because of the inherent shortcoming of transient absorption (TA) spectroscopy. One way to overcome this issue could be to use two-dimensional (2D) electronic spectroscopy in order to get information about the phase, which is necessary as a feedback signal in coherent control experiments. However, multidimensional spectroscopy is not the only possible approach.

Here we solve this issue by using an open-loop control approach: one first numerically optimizes laser pulses via numerical simulations and the applies them to the sample obtaining the desired result, for example, the experimental preparation of the sample in some desired state with very high fidelity. The main advantages of the open-loop approach with respect to the closed-loop approach are twofold. In the latter, the pulses are often very complex, highly structured, and very demanding to interpret; it is usually rather difficult to understand the real physical effect of such series of consecutive pulses on the system. This limits the understanding of the physical processes underlying a given biological behavior. Moreover, repeated closed-loop experiments rarely result in the same genetic algorithm-driven learning curve, increasing the difficulties of the analysis of the final optimal series and of the error estimation. On the other hand, in the open-loop scheme, the optimally shaped pulse is well determined and can be applied on the sample repeatedly to increase the signal-to-noise level and to compare the output feedback when changing the applied phase. It is then easier to find the explanation for the response of the system and identify the physical mechanism that underpins it. This problem becomes even simpler when the CRAB optimization is used since, as explained below, it results in optimal, albeit very simple, robust and structured pulses. Let us stress, however, that the open-loop technique is usually applied when the system parameters (e.g., Hamiltonian) are sufficiently well known and this, indeed, makes the closed-loop approach more feasible for those biological systems in which this information is not yet accessible. In this context, recently developed methods for quantum process tomography applied to multichromophoric systems [24], providing the decoherence of the system, the density matrix, as well as the Hamiltonian parameters, will be able to assist our open-loop approach. This is even more so as the robustness of the pulse shapes that we obtain from our open-loop technique allow us to use this scheme even if the system details are not well measured. Quite reasonably, the best scheme would be a combination of these two approaches. Indeed, one could use, for instance, closed-loop control as a means to obtain information about system parameters, e.g., if one optimizes the pulse in the experiment, then one can chose this pulse and find out theoretically for which system parameters it reproduces the experimental data. Then, varying the target that is to be optimized, we obtain different pulses and can repeat this investigation; each time, one obtains useful information about the system parameters. Working out such a program might be useful as it might allow for an alternative to tomography. Once we apply this procedure, by using the obtained information about the system, an open-loop control can be then successfully applied. A work applying open-loop optimal control to the FMO complex was reported in [18]. The authors investigate the control of FMO exciton dynamics by using polarized-shaped pulses optimized by means of a derivative functional equation for the target function. In particular, they use shaped pulses to optimize energy localization in a single chromophore of the FMO complex (site 7).

Here we extend and improve this result by using the recently developed CRAB optimization technique (described below) targeting different initial states, to investigate different transport and decoherence processes in FMO. Moreover, we are able to consider faster processes that are more robust against decoherence as we optimize pulses of a few-hundred-femtosecond length. This allows us also to perform coherent control, i.e., preparation of a coherent superposition state, as well as excitation energy localization. Concerning the case of single-site preparation, it is not feasible to perform a clear comparison with the results of Ref. [18], since they studied the FMO antenna complex present in the *Chlorobium tedidum* bacterium, while here we investigate the FMO complex found in a slightly different bacterium, *Prosthecochloris aestuarii*. However, from a general perspective, it seems that our approach allows us to get much higher fidelity, and, more

importantly, to use sensibly shorter laser-pulse lengths (250 fs, while their optimal pulses are 600 fs long). These differences appear to be even more relevant and crucial when one wants to prepare a coherent superposition state in the presence of strong dephasing. Besides, the efficiency of the CRAB algorithm makes it possible to investigate more deeply inhomogeneous broadening phenomena, due to the random orientations of the FMOs in the sample, by considering very large ensembles (10^4 FMOs); while in Ref. [18], due to computational limitations, only some preliminary results were reported. In fact, we demonstrate that even a partial orientation of the sample by means of an external field combined with optimal pulses will improve experimental results significantly. Finally, we show also how to optimize the probe of the system to improve the experimental results even more. It should be noted that since we are considering short pulse durations, neglecting the double-exciton states is a good approximation, also according to the theoretical results in Ref. [18]; see discussion below about the robustness of our weak pump pulses.

To achieve all of this, we use the Chopped RAndom Basis (CRAB) optimization, introduced in Ref. [19], to optimize a specific figure of merit $\mathcal{F}$, e.g., the population in some localized or delocalized state at some final time or the final fidelity with respect to a target state, by varying the control field entering into the Hamiltonian term in Eq. (4). By introducing the control field parametrization given in Eq. (5), the functional becomes a multivariable cost function $\mathcal{F}(\Delta\theta,\Delta\phi,\omega_l,t_0,\sigma,\{A_k\},\{B_k\},\{\nu_k\})$ on which any standard minimization method can be applied. We start with $O(10^3)$ different initial random configurations and apply a direct search algorithm, which does not compute gradient nor Hessian, to find the function minimum [25]. To minimize an M-variable function, the Nelder-Mead algorithm starts defining an $M+1$ dimensional polytope and then, in its simplest implementation, moves it, replacing the worst point with a point reflected through the barycenter of the other M points, resulting in a (local) minimization of the function. We use the subplex variant of the Nelder-Mead algorithm, which applies the same algorithm to different subspaces to improve the convergence [26]. The CRAB optimization strategy introduced above allows one to find the optimal pulses to extremize the desired figure of merit: it is efficient and versatile as it does not need any analytical solutions of the system dynamics, it does not compute gradients, and it can be easily adapted to different figures of merit. More importantly, it could include experimental constraints such as the finite bandwidth and power of the control pulses.

III. THE MODEL

The *coherent* part of the dynamics of the FMO complex can be modeled by a 7-qubit (Frenkel) Hamiltonian describing the coherent exchange of excitations between chromophores or sites, i.e.,

$$H_{\mathrm{FMO}} = \sum_{j=1}^{7} \hbar\omega_j \sigma_j^+ \sigma_j^- + \sum_{j\neq l} \hbar v_{j,l} (\sigma_j^- \sigma_l^+ + \sigma_j^+ \sigma_l^-),$$

where σ_j^+ (σ_j^-) are the raising (lowering) operators for site j, $\hbar\omega_j$ is the local site excitation energy, and $v_{j,l}$ (of the order

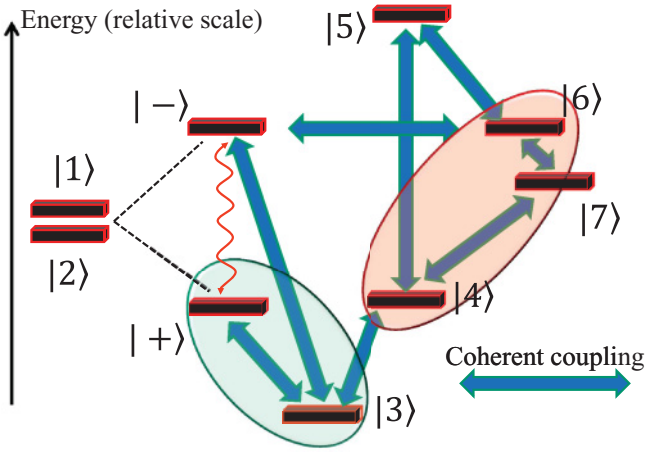

FIG. 1. (Color online) FMO energy-level structure where $|i\rangle$ denotes a single excitation in site i. The states $|\pm\rangle$ are the symmetric and antisymmetric superpositions of the states $|1\rangle$ and $|2\rangle$. The green (light gray) and red (dark gray) bubbles identify the fast and slow transport path, as detailed in Ref. [10] where the interplay between different transport pathways in FMO dynamics was discussed at length. The main effect of the inclusion of dephasing noise is the opening of an incoherent relaxation channel from level $|-\rangle$ to level $|+\rangle$ (red wiggled line) and therefore the effective suppression of the coherent oscillation between level $|-\rangle$ and sites 6-7-4 that dominates the coherent dynamics and is responsible for the very slow transport once the sink population has reached 50% (initial population held in site $|+\rangle$). The proposed quantum control strategies efficiently probe this dynamical model.

of ps^{-1}) denotes the hopping rate of an excitation between the sites j and l; see Ref. [8] for more detail. In the site basis, the Hamiltonian matrix elements [27] are

$$H = \begin{pmatrix} 215 & -104.1 & 5.1 & -4.3 & 4.7 & -15.1 & -7.8 \\ -104.1 & 220.0 & 32.6 & 7.1 & 5.4 & 8.3 & 0.8 \\ 5.1 & 32.6 & 0.0 & -46.8 & 1.0 & -8.1 & 5.1 \\ -4.3 & 7.1 & -46.8 & 125.0 & -70.7 & -14.7 & -61.5 \\ 4.7 & 5.4 & 1.0 & -70.7 & 450.0 & 89.7 & -2.5 \\ -15.1 & 8.3 & -8.1 & -14.7 & 89.7 & 330.0 & 32.7 \\ -7.8 & 0.8 & 5.1 & -61.5 & -2.5 & 32.7 & 280.0 \end{pmatrix},$$

where the zero of energy has been shifted by 12 230 cm^{-1} for all sites, corresponding to a wavelength of $\cong$800 nm (all numbers are given in units of $\mathrm{cm}^{-1} = 1.988865 \times 10^{-23}$ Nm $= 1.2414 \times 10^{-4}$ eV); see Fig. 1.

In a first approximation, the evolution of the complex can be modeled in terms of a master equation of the Lindblad form including dissipation and pure dephasing terms due to the surrounding environment. This approach is equivalent to the so-called Haken-Strobl model, where pure dephasing is taken into account in terms of a classical fluctuating field [28]. Although it is a simplistic description of the realistic dynamics, it allows us to prepare the ground for such control experiments showing their feasibility and will suffice for the identification of coarse-grained properties of the transport dynamics.

The dissipation and dephasing caused by the surrounding environment are modeled by the following local Lindblad

terms:

$$\mathcal{L}_{\rm diss}(\rho) = \sum_{j=1}^{7} \Gamma_j [-\{\sigma_j^+\sigma_j^-,\rho\} + 2\sigma_j^-\rho\sigma_j^+], \qquad (1)$$

$$\mathcal{L}_{\rm deph}(\rho) = \sum_{j=1}^{7} \gamma_j [-\{\sigma_j^+\sigma_j^-,\rho\} + 2\sigma_j^+\sigma_j^-\rho\sigma_j^+\sigma_j^-], \qquad (2)$$

with Γ_j and γ_j being the dissipative and dephasing rates at the site j, respectively. In the following, we will consider the case in which the dephasing and dissipation rates are equal for all sites and labeled, respectively, as $\gamma_j \equiv \gamma$ and $\Gamma_j = 5 \times 10^{-4}$ ps^{-1} for site $j = 1, \ldots, 7$. The latter corresponds to the measured lifetime of excitons, which is of the order of 1 ns. Finally, the transfer efficiency into the reaction center (RC) is measured in terms of the population in the "sink," numbered 8, which is populated by an irreversible decay process (with rate $\Gamma_{\rm sink}$) from the site 3, as described by the Lindblad term

$$\mathcal{L}_{\rm sink}(\rho) = \Gamma_{\rm sink}[2\sigma_8^+\sigma_3^-\rho\sigma_3^+\sigma_8^- - \{\sigma_3^+\sigma_8^-\sigma_8^+\sigma_3^-,\rho\}], \qquad (3)$$

where $\Gamma_{\rm sink} \sim 6.3$ ps^{-1} (note that $\hbar \sim 5.3$ cm^{-1} ps). In this paper, we are interested in the EET transfer efficiency, as measured by the population (after a certain time interval) of a trapping site, modeling a biochemical reaction center (RC). The RC is populated by an irreversible decay process from site 3, and the RC population will allow us to define fast and slowly evolving states. In other terms, the transfer efficiency is given by $p_{\rm sink}(t) = 2\Gamma_{\rm sink}\int_0^t \rho_{33}(t')dt'$, with $\rho_{33}(t')$ being the population of site 3 at time t'; see inset of Fig. 2.

In order to describe the coupling between the FMO complex and a short laser pulse, typically used in the laboratory to irradiate it [2,27,29,30], we add also a semiclassical time-dependent Hamiltonian term, $H_{\rm FMO-laser}(t)$, which in rotating wave approximation takes the form

$$H_{\rm FMO-laser}(t) = -\sum_{i=1}^{7} \vec{\mu}_i \cdot \vec{e}\; E(t)\, e^{-i\omega_l t}\, \sigma_i^+ + \text{H.c.}, \qquad (4)$$

where $\vec{\mu}_i$ is the molecular transition dipole moment of the individual site i [31], $\vec{e}$ and ω_l are, respectively, the polarization and the frequency of the field, and $E(t)$ is the time-dependent electric field. In the following, we assume $E(t)$ having the form

$$E(t) = E_0 f(t),$$

with $E_0 = 15$ D^{-1} cm^{-1} $\sim 9 \times 10^7$ V/m (where in SI units the Debye is given by $D \sim 3.34 \times 10^{-30}$ C m), and a time-dependent modulation

$$f(t) = \frac{e^{-\frac{(t-t_0)^2}{2\sigma^2}}}{\lambda(t)} \frac{1 + \sum_{k=1}^{m} A_k \sin(\nu_k t) + B_k \cos(\nu_k t)}{1 + \sum_{k=1}^{m} |A_k| + |B_k|}, \qquad (5)$$

with a ramp factor of $\lambda(t) = 1 + 5[e^{200(t-T)/T} + e^{-200t/T}]$ [such that $f(0) \sim f(T) \sim 0$], and where A_k, B_k, and $\nu_k \equiv 2\pi k r/T$ are parameters to be optimized by using the method described below, where r is a random number and T is the time at which we want to prepare, for instance, some desired state. Moreover, we vary also the angles θ and ϕ of the polarization axis $\vec{e}$, with respect to the dipole moment of site 1, i.e., $\theta = \theta_1 + \Delta\theta$ and $\phi = \phi_1 + \Delta\phi$, where θ_1 and ϕ_1 describe the orientation of the site-1 dipole moment, and $\Delta\theta$ and $\Delta\phi$ are some free parameters. The dipole moments of the seven FMO chromophores along the three reference axes are (in Debye D, where $1D \sim 3.34 \times 10^{-30}$ C m) [31] shown in the table below for the bacteriochlorophyll (BChl).

BChl	X	Y	Z
1	− 3.081	2.119	− 1.669
2	− 3.481	− 2.083	− 0.190
3	− 0.819	− 3.972	− 0.331
4	− 3.390	2.111	− 1.080
5	− 3.196	− 2.361	0.7920
6	− 0.621	3.636	1.882
7	− 1.619	2.850	− 2.584

Note that the specific choice of the absolute strength of the dipole moments (usually set to be the same for each BChl) does not affect our results because it does correspond to simply rescale the laser pulse amplitudes, as discussed below. In the following, we choose $m = 7$, $T = 250$ fs, and the carrier frequency ω_l as an additional free parameter in the optimization. We have also worked with higher values of m, up to $m = 25$, which resulted in small fidelity enhancements (of a few percent), but at the expense of longer optimization times. As direct single-site addressing is not possible in the FMO complex due to the strongly overlapping lines, we will apply quantum optimal control tools (as described more carefully in the next section) to shape the laser pulse, i.e., $E(t)$, and prepare the system in a desired physical state and control its transport dynamics. The approach presented here allows one to include additional constraints to account for relevant experimental limitations: we limit, for example, the laser power in order to avoid damage to the sample or cause strong saturation; and we impose that the spectral width of the pulse does not exceed 0.1 fs^{-1}, which is commensurate with standard experimental settings.

IV. OPTIMIZATION TARGET

A typical experiment will excite the complex with a Gaussian laser pulse resulting in population of all sites due to lack of control and single-site addressability. Here, we implement quantum control using the CRAB algorithm [19] for optimal preparation—without single-site addressing—of *arbitrary* states, localized or delocalized, by varying the control laser-field amplitude, carrier frequency, and polarization axis. In Ref. [10], it has been shown that the coherent transfer of the electronic excitation energy in the FMO complex can be neatly understood in terms of a hybrid basis that includes delocalized states $|\pm\rangle = (|1\rangle \pm |2\rangle)/\sqrt{2}$ and local states $|i\rangle$ ($i = 3, \ldots, 7$); see Fig. 1. Transport takes place essentially through two different pathways: one mediated by the state $|+\rangle$, which is shifted toward site 3 and leads to very fast transfer to the RC, and a second one, involving the remaining part of the initial excitation that is held in state $|-\rangle$ and the sites 5, 6, and 7, which is comparatively slow because of the energy gap with the site 3 and because the excitation suffers many coherent oscillations between those sites before reaching site 3. Indeed, the presence of dephasing noise assists the transport because, on one hand, it opens up a new additional pathway, i.e., incoherent tunneling between the state $|-\rangle$ and $|+\rangle$, and, on the other hand, it partially suppresses the transition from $|-\rangle$

to sites 5, 6, and 7, and also leads to fast incoherent oscillations between those three sites before reaching the RC. Motivated by these results, we apply the CRAB optimization to find the optimal pulses to selectively prepare after 250 fs, on one hand, a state $|D\rangle$ with maximum probability of finding the electronic excitation in the sites $|5\rangle,|6\rangle,|7\rangle$ (*dark* or nonpropagating state), and, on the other hand, the state $|B\rangle \equiv |+\rangle$ (*bright* or propagating state) with maximal fidelity. Our figures of merit are the following error probabilities:

$$\varepsilon_D = 1 - \rho_{5,5} - \rho_{6,6} - \rho_{7,7}, \tag{6}$$

$$\varepsilon_B = 1 - \langle +|\rho|+\rangle = 1 - \frac{\rho_{11} + \rho_{22}}{2} - \mathrm{Re}[\rho_{12}], \tag{7}$$

where ρ is the FMO density matrix in the site basis. They represent the error probabilities for preparing the system in some specific initial state (e.g., state D or B). In the following, we will consider different values of dephasing, i.e., different noise regimes, and for each of them we will perform a coherent control optimization, obtaining a different error ϵ_α. We consider the full model for the FMO complex, but in the absence of the RC, as this is the usual setting in current experiments on this light-harvesting system. However, we have tested that the presence of the RC does not affect significantly the state preparation process because the laser pulse is applied for a very short time. This is also confirmed by the analysis on the transport pathways discussed below.

Finally, let us point out that we are neglecting third-order contributions to the density matrix in terms of the system-field interaction, like ground-state bleaching (GBS) and excited-state absorption (ESA) processes. This approximation is justified by the fact that we are considering the density matrix in the single-exciton subspace (which is second order) and, then, those higher-order terms are not relevant for the pump-pulse optimization.

V. OPTIMAL PULSES FOR SINGLE MOLECULES

In the case of single molecules or oriented samples, we find that the error ε_α without dephasing is of the order of a few percent and increases in both cases when increasing the amount of dephasing in the dynamics; see Fig. 2. The so-derived weak pulses are also robust against changes in system parameters and environmental noise levels. This general feature (see, e.g., [32,33]) arises from the fact that by definition the optimal dynamics lies in a minimum of the functional to be extremized, so that first-order perturbations vanish. Indeed, we find that the optimality of the pulse shape that prepares some desired state is essentially independent of the strength of the dephasing noise in the dynamics, with an error discrepancy of less than 10^{-2}. This is very relevant from the experimental point of view, since the noise strength in the actual FMO complex is not yet precisely known and depends on the specific experimental conditions. In addition, linearized optimal pulses (see insets of Fig. 4) give similar results, whose difference is less than 0.05 for both states.

Importantly, our optimal errors remain exactly the same (i.e., standard deviation smaller than 10^{-3}) if we reduce the obtained amplitudes (already similar to the ones in Ref. [18]) by a factor up to 1000, while keeping the pulse shapes, carrier frequencies, and polarization at their optimal values. In other words, our results are very robust and are valid in the weak-field domain, allowing us to neglect undesired effects induced by strong lasers, such as ladder-climbing effects (inducing unwanted photochemical processes), excitation of double-exciton states, ground-state bleaching, stimulated emission, etc. In particular, we have performed the following analysis. First, note that from the experimental side, the physically relevant quantities are not the absolute site populations, but only the relative ones, as compared to the ground state (gs). In other words, we can rescale the density matrix with $1 - \rho_{\mathrm{gs}}$, with ρ_{gs} being the ground-state population, and then evaluate the errors. It turns out that these rescaled errors are even smaller (hence, higher fidelities) than the ones shown in Fig. 2. Furthermore, we have rescaled our optimally shaped pulses (in the insets of Fig. 4) by a factor of $1/R$, i.e., reducing the laser amplitude by increasing R, while keeping the same pulse shape and the other optimal parameters, as polarization and carrier frequency. The very interesting result is that the rescaled errors are exactly the same for any $R = 1, \ldots, 1000$; see Fig. 3. In

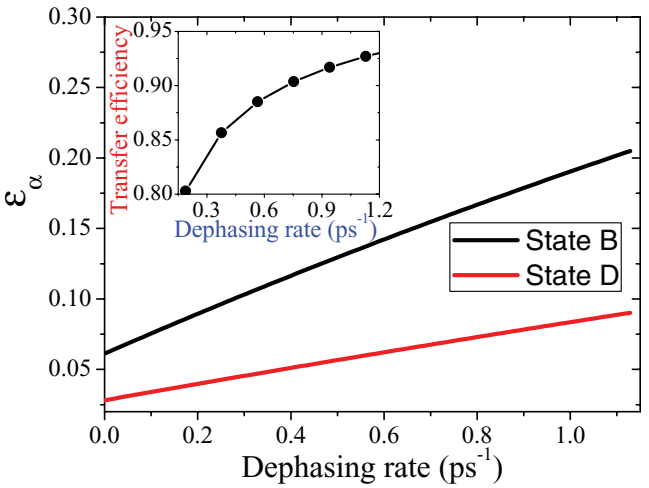

FIG. 2. (Color online) Error probability ε_α vs dephasing rate γ (in units of ps^{-1}) for different initial states (i.e., $\alpha = B,\ D$). Inset: Transfer efficiency vs dephasing rate γ (uniform for all of the sites) at $t = 10$ ps, when one excitation is initially in site 1.

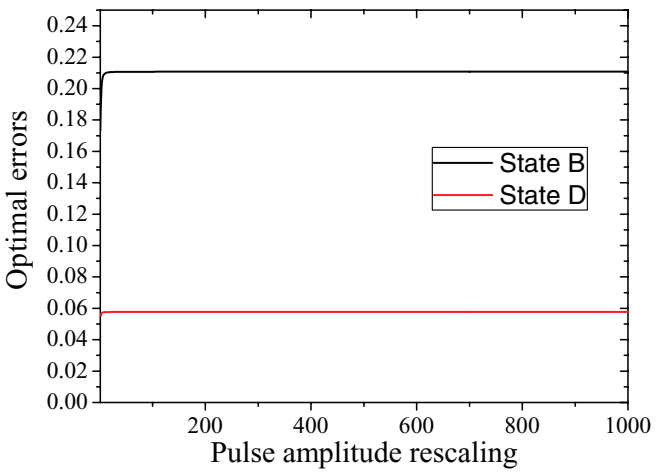

FIG. 3. (Color online) Optimal errors $\epsilon_{B,D}$ vs the pulse amplitude rescaling (R) in the preparation of the initial states B and D, for $\gamma \sim 1$ ps^{-1}.

other words, even using much weaker pulses, our achievements remain the same, showing the surprisingly strong robustness of our initial state preparations against the actual laser amplitude. Therefore, we propose to use very weak pulses and this will further simplify the experimental realization of our biocontrol scheme.

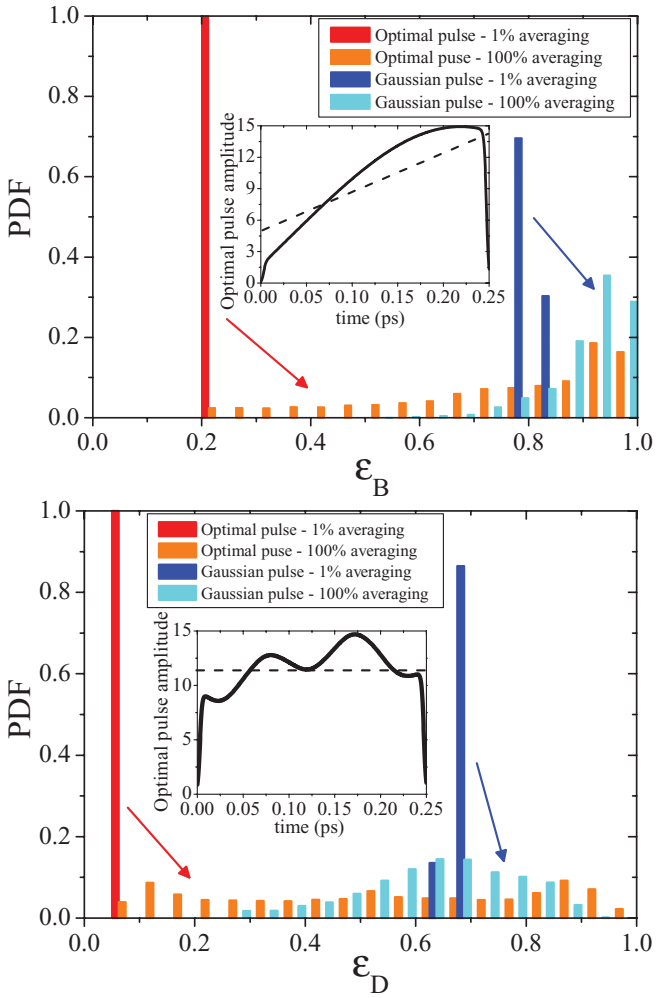

FIG. 4. (Color online) Probability distribution of the quantity ε_B (top) and ε_D (bottom) for the preparation of the state *bright* B (top) and the state *dark* D (bottom), in the presence of dephasing with rate $\gamma \sim 1\ \mathrm{ps}^{-1}$, by using the optimal and a standard Gaussian laser pulse. Since in the laboratory one has a sample of FMO complexes in random orientations, we plot these probability distribution functions (PDFs) for two extreme cases in which we add 1% and 100% of random disorder to the two angles defining the orientation of the FMO complex. We considered a sample of 10^4 FMO complexes to get enough statistics. Inset: Amplitude of the optimal pulse, optimized to prepare the state B (top) and D (bottom) in 250 fs. Notice that the laser-pulse amplitude is always shown in units of $\mathrm{D}^{-1}\,\mathrm{cm}^{-1} \sim 6 \times 10^6\ \mathrm{V/m}$. Finally, the optimal values are (top) $\Delta\theta = 2.5$, $\Delta\phi = 7.6$, $\omega_l = 121.76\ \mathrm{cm}^{-1}$, $\varepsilon_B = 0.20$, without averaging, and (bottom) $\Delta\theta = 3.09$, $\Delta\phi = 3.76$, $\omega_l = 504.46\,\mathrm{cm}^{-1}$, $\varepsilon_D = 0.09$, without averaging. Interestingly enough, by considering a simpler linear shape (dashed line), we find a quite similar error, i.e., $\varepsilon_B = 0.24$ and $\varepsilon_D = 0.10$, by showing the "robustness" of the optimal pulse to prepare the initial state.

Notice also that by removing some of the experimentally motivated constraints on the pulse shape, it is possible to find near unit fidelity for any state and any value of the dephasing rate: future experiment with improved technical capabilities will easily result in higher quality of the initial state.

VI. OPTIMAL PULSES FOR DISORDERED ENSEMBLES

Here we characterize the probability distribution functions concerning the optimal preparation of the initial state in the case of randomly oriented FMO complexes. We apply the optimal pulses found for a single FMO complex (shown in the insets of Fig. 4) to an ensemble of 10^4 FMO complexes with random (uniform distribution) orientations, $\theta \in [0,\pi]$ and $\phi \in [0,2\pi]$. The results are illustrated in Fig. 4, where the error distributions for the optimal case and the initial Gaussian pulse are compared. In the case of the state B analyzed in Fig. 4 (top), the ensemble averages of ε_B are 0.207 and 0.751, respectively, for 1% and 100% of orientation disorder, in the case of the optimal pulse, while they are 0.793 and 0.904 in the Gaussian one, respectively. On the other hand, for the state D analyzed in Fig. 4 (bottom), the distribution averages are, respectively, 0.091 and 0.531 in the case of the optimal pulse,

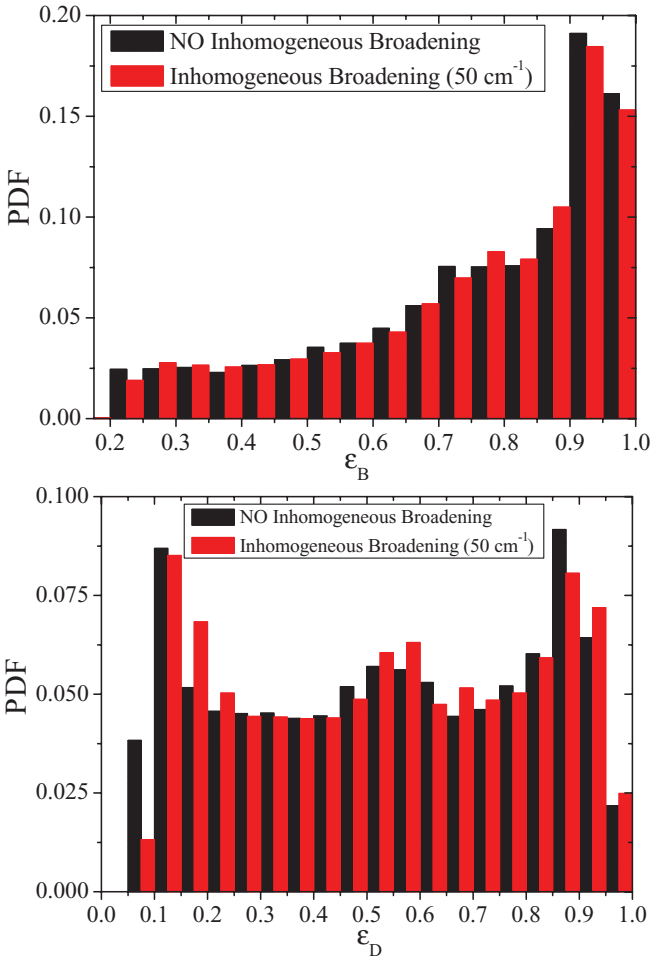

FIG. 5. (Color online) Probability distribution of the quantity ε_B (top) and ε_D (bottom), for the preparation of the states B and D, respectively, in the case of 100% orientation disorder, in the presence and absence of inhomogeneous broadening (set to $50\ \mathrm{cm}^{-1}$).

and 0.663 and 0.634 in the Gaussian one. The optimal pulses give a significant improvement also in the case of randomly oriented FMO complexes, appearing pretty robust with respect to large inhomogeneities of the system. This robustness is also witnessed by the fact that in the case of a single FMO, by considering a simpler linear pulse shape (interpolating the optimal one; see dashed line in the inset of Fig. 4), a very similar error is obtained, whose difference is less than 0.05 in both cases (D and B states).

Finally, we test the robustness of the obtained optimal pulses with respect to the presence of inhomogeneous broadening, i.e., static disorder in the site energies. In particular, we have considered an inhomogeneous broadening of 50 cm^{-1}, corresponding to a random shift in the scale of [0, 50] cm^{-1} to the site energies, but different for each site. We find that in the presence of 100% orientation disorder, the error distributions for site B and D, as in Fig. 4, are not affected from inhomogeneous broadening; see comparison in Fig. 5. In particular, the mean and the variance of the corresponding distributions are equal within a difference of 10^{-2}.

VII. TRANSFER EFFICIENCY: SINGLE MOLECULE AND ENSEMBLE

We now compare the EET transfer efficiency corresponding to the two different initial states D and B optimally prepared by our laser pulses. The ratio of the fast and slow pathway transfer efficiency, at time $t = 2$ ps, is about 2.5 for $\gamma \sim 1$ ps^{-1}, while it reaches about 80 for $\gamma = 0$, as shown in Fig. 6 and expected from the fact that dephasing reduces destructive interference effects [8]. These results are particularly robust against various possible experimental inaccuracies. Indeed, in Fig. 6, we show that although state preparation by the optimal laser pulse is not perfect, the corresponding behavior is still sufficient to distinguish the slow and fast transport pathways, compared to the case in which the specific states are initially exactly set in

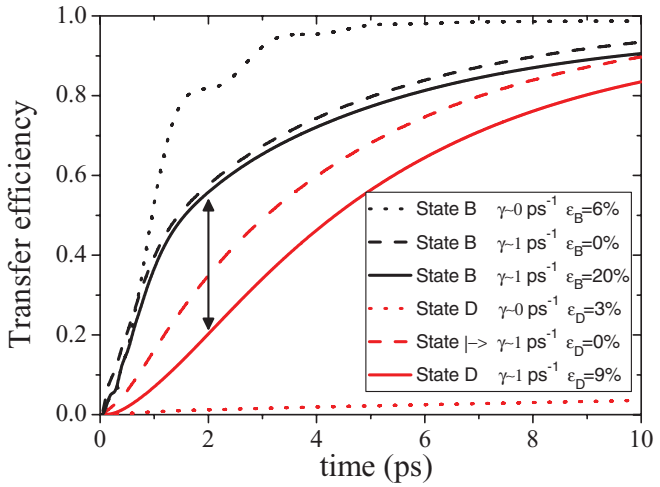

FIG. 6. (Color online) Transfer efficiency as a function of time (ps) for different initial states. We consider an idealized preparation of the states $|-\rangle$ and $|B\rangle$, i.e., $\varepsilon_\alpha = 0$ (dashed lines), and a more realistic scenario where the states $|D\rangle$ and $|B\rangle$ are prepared applying the optimally shaped laser pulses, in the absence (dotted lines) and presence (full lines) of dephasing noise, $\gamma \sim 1$ ps^{-1}.

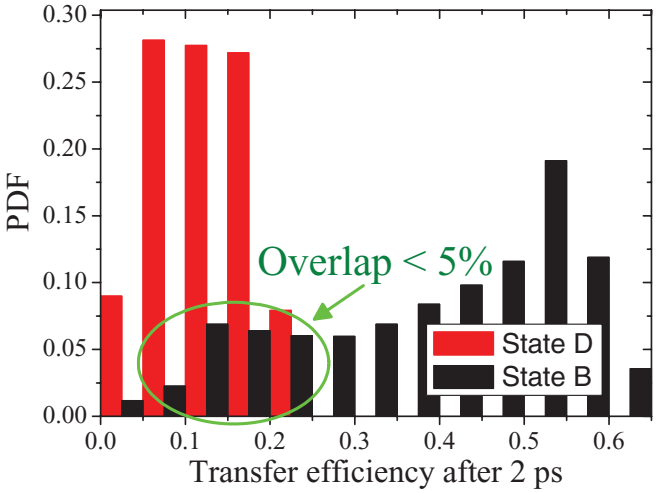

FIG. 7. (Color online) Probability distribution of RC transfer efficiency after 2 ps, in the presence of local dephasing with rate $\gamma \sim 1$ ps^{-1}, for the optimal preparations of the state D and the state B, with 100% of random disorder in the orientation of 10^4 FMO complexes. The two distributions are distinguishable with less than 5% error.

the numerical simulation. This fact is essential to reproduce these results in the laboratory since the experimental fidelities will be smaller than the theoretical ones.

Moreover, as above, we also consider a realistic experimental scenario in which a very large ensemble of FMO molecules is studied simultaneously in the laboratory with different random orientations. It turns out that even with 100%

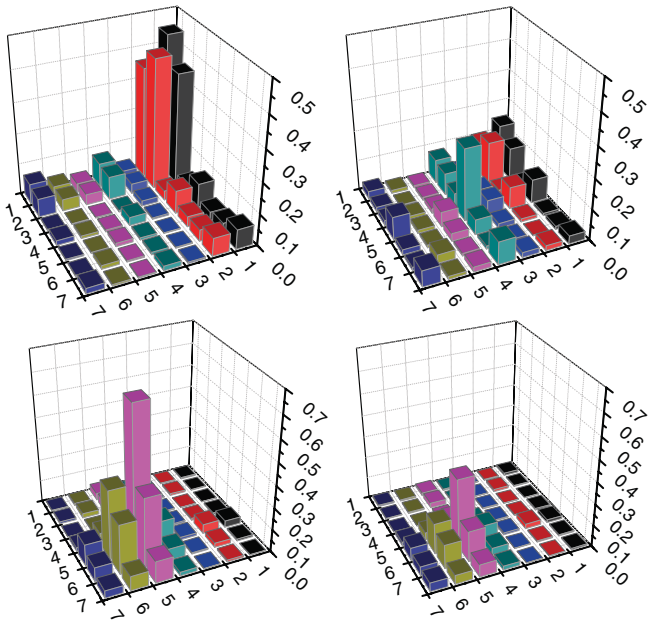

FIG. 8. (Color online) Modulus of the ensemble average of the elements of the FMO density matrix in the site basis (over 10^4 samples), after applying the optimally shaped laser pulse to prepare the states B (top) and D (bottom), for $\gamma \sim 1$ ps^{-1}. We introduce also orientation disorder, set to 1% (left) and 100% (right), and we get the following errors: $\varepsilon_B = 0.21$ (top left), $\varepsilon_B = 0.75$ (top right), $\varepsilon_D = 0.09$ (bottom left), $\varepsilon_D = 0.53$ (bottom right).

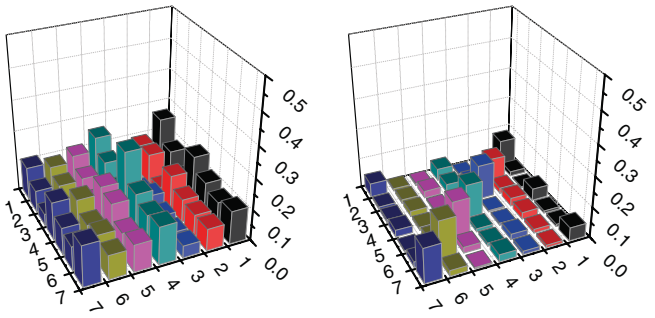

FIG. 9. (Color online) Modulus of the ensemble average of the elements of the FMO density matrix in the site basis (over 10^4 samples), after applying a standard Gaussian pulse, for $\gamma \sim 1$ ps^{-1}. We consider also the presence of orientation disorder, which is set to 1% (left) and 100% (right), respectively.

random disorder in the orientations of the FMO molecules, the difference between the transfer efficiencies after 2 ps of the *dark* and *bright* states is still measurable. Indeed, as shown in Fig. 7, the two distributions of transfer efficiency are distinguishable with less than 5% error, estimated as the sum of the products of corresponding probabilities in the overlapping range. The ensemble averages are around 0.12 in the case of the state D, and 0.39 for the state B.

The modulus of the ensemble average of the elements of the FMO density matrix in the site basis, after the state preparation by means of the optimal pulse and the Gaussian one, are shown in all of the analyzed cases (in the presence of orientation disorder) in Figs. 8 and 9. Let us stress that a partial orientation of the sample allows one to significantly improve the state preparation results shown above. Indeed, a net improvement is observed in Fig. 10, when compared to the 100% disorder case shown in Figs. 8.

Therefore, this analysis demonstrates that the difference in physical behavior should be observable in a real experiment. This type of analysis can be also extremely useful for the discrimination of different microscopic models used in the inference of site energies and electronic couplings from molecular dynamics analysis [27] or from directly measurable exciton energies [34].

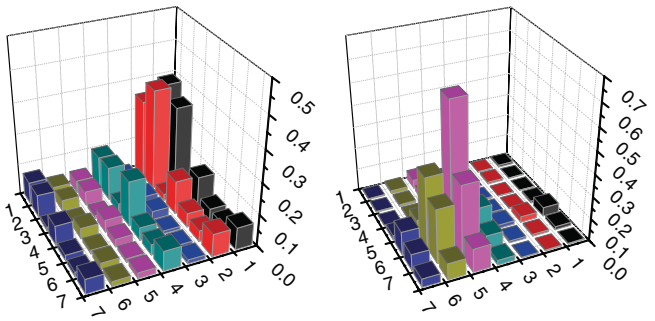

FIG. 10. (Color online) Modulus of the ensemble average of the elements of the FMO density matrix in the site basis (over 10^4 samples), after applying the optimally shaped laser pulse to prepare the states B (left) and D (right), respectively, for $\gamma \sim 1$ ps^{-1}, and orientation disorder set to 10% in both cases, considering that some orientation will be obtained in the experiment. The errors are $\varepsilon_B = 0.44$ and $\varepsilon_D = 0.10$, respectively.

VIII. DISORDER-BASED OPTIMIZATION

In the analysis above, the optimization has been performed by considering a single FMO complex and then applying the optimal pulses to a realistic sample containing many FMOs. However, optimizing the laser pulse taking into account the presence of orientation disorder might improve our results. In order to cover almost isotropically the different orientations of the photosynthetic system in the sample, we optimize the pulse, minimizing the quantity ε_α averaged over a sample of 20 FMO complexes oriented along the directions pointing to the 20 vertices of a dodecahedron. In Fig. 11, we show the probability distribution for ε_D when this new optimal pulse is applied to a sample of 10^4 FMOs in random orientations. For comparison, we plot also the corresponding probability distribution when we instead apply the optimal pulse computed with a single orientation. It turns out that this new pulse is more robust and provides an error distribution whose width is about one half of the one obtained with the pulse optimized with a single FMO system. This could suggest a way to improve the state preparation of the FMO complex in a real experiment where one has a sample containing many FMO molecules in a solution. However, concerning the preparation of the more delicate state B, this technique does not provide any noticeable improvement. Moreover, regarding the transport properties, the results are similar to those presented in Fig. 7,

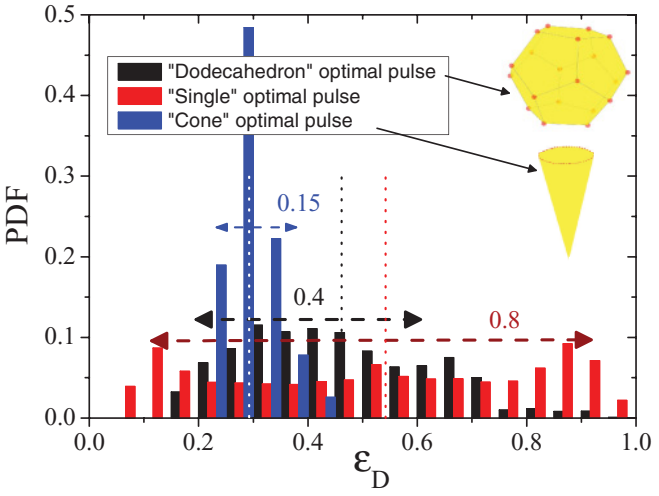

FIG. 11. (Color online) Probability distribution of the quantity ε_D for the preparation of the state D, for $\gamma \sim 1$ ps^{-1}, by using the optimal pulses obtained by considering a single FMO complex, by averaging on a small sample of 20 (almost isotropic) FMO orientations pointing to the 20 vertices of a dodecahedron, and on a sample of 21 orientations inside a cone with an opening angle of 0.1π. Hence, one considers the probability distribution of ε_D when these optimal pulses are applied to a sample of 10^4 FMO complexes in completely random orientations in the first two cases and, for the last case, randomly oriented inside that cone. The dashed lines represent the corresponding averaged values, i.e., 0.53 (single orientation), 0.46 (dodecahedron), and 0.29 (cone). The corresponding distribution widths are also plotted.

and the overlap of those two distributions is still less than 5% but does not decrease any further. Notice that this overlap is already rather small and so the two pathways should be experimentally clearly distinguishable. Finally, we consider an intermediate case in which the FMO complexes can be partially oriented along a cone-shaped range of orientations. In particular, we repeat the analysis above but for 21 directions inside a cone with a 10% opening angle, i.e., 0.1π, and we optimize the pulse, minimizing the quantity ε_α averaged over 21 FMO complex evolutions. Then we apply this optimal pulse to a sample of 10^4 FMOs in random orientations inside this cone and we calculate the probability distribution for ε_D; see Fig. 11. We find that the width of the error distribution is further squeezed and shifted to smaller errors, i.e., higher fidelities.

IX. TOWARD ORIENTED SAMPLES

Several techniques have been proposed in literature in order to align biological molecules, for instance by using strong laser pulses [35], liquid crystals [36], stretched gels [37], and optical tweezers [38]. Here we show just a simple argument providing the rudiments of how one could try to orientate the FMO systems in an experimentally available sample. Following Ref. [39], we model each monomer of the FMO complex as a disk, whose mass and radius can be reasonably estimated to be equal to $M \sim 80$ kDa $\sim 15 \times 10^{-23}$ kg and $R = 2$ nm (including the protein scaffolding). The corresponding moment of inertia (with respect to one of its diameters as the rotational axis) is hence $I = \frac{1}{4}MR^2 \sim 1.125 \times 10^{-31}$ kg m^2. The rotational energy is $E = \frac{1}{2}I\omega^2$, with ω being the angular velocity in radians per second, i.e., the derivative of the angle rotated with respect to time $\omega = \frac{d\theta}{dt}$. At room temperature, neglecting the friction due to the presence of a solution and, possibly, other more sophisticated effects, just to get an initial rough estimation, the time $t_{\rm rot}$ it takes for the system to rotate by an angle $\pi/2$ (which is roughly the average angle by which a complex has to be rotated) is trivially given by $t_{\rm rot} = \frac{\pi}{2}\sqrt{\frac{I}{2E_{\rm th}}} \sim 6$ μs, with $E_{\rm th} \sim 25$ meV as the thermal energy. Actually, given that the disk will carry out a sort of random walk, the rotation time could be much longer than what is estimated here by means of this simple analysis. Moreover, we investigate the energy landscape as a function of the orientation of the FMO complex, when it is subject to a constant electric field E_0 polarized along the axis $\vec{e}$ with carrier frequency ω_l, i.e., the following quantity:

$$\Delta = \sum_{i=1}^{7} \frac{|\vec{\mu}_i \cdot \vec{e}\, E_0|^2}{\omega_i - \omega_l}. \tag{8}$$

By varying the orientation of the FMO complex in terms of the two angles θ and ϕ, the energy difference between the maximum and the minimum value is comparable to the thermal energy and one gets the maximum for $\Delta\theta \sim 1.75$ and $\Delta\phi \sim 2$; see Fig. 12. The other parameters are chosen as $\omega_l = -1000$ cm^{-1} and $E_0 = 40$ D^{-1} cm^{-1}.

Finally, following the simple reasoning above, we explicitly calculate how many FMO systems can be oriented around some direction at a certain external temperature, since the thermal fluctuations will unavoidably try to disorientate the sample. To do this, we calculate the probability for the FMO to be oriented at a certain angle by assuming that they follow a Boltzmann-Gibbs distribution, in the presence of a constant electric field; see bottom panel in Fig. 13. Then, by using the obtained probability distribution, we also evaluate the fraction of FMO systems oriented within a cone with a certain opening angle as a function of the temperature and for different values of opening angle. By decreasing the temperature, the amount of oriented FMO systems in the sample increases, and this would give us higher fidelities in the state preparation analysis and for the other related results above. Therefore, it seems feasible to orientate the FMO complexes in the sample to some extent using far detuned laser light. The typical individual optimal

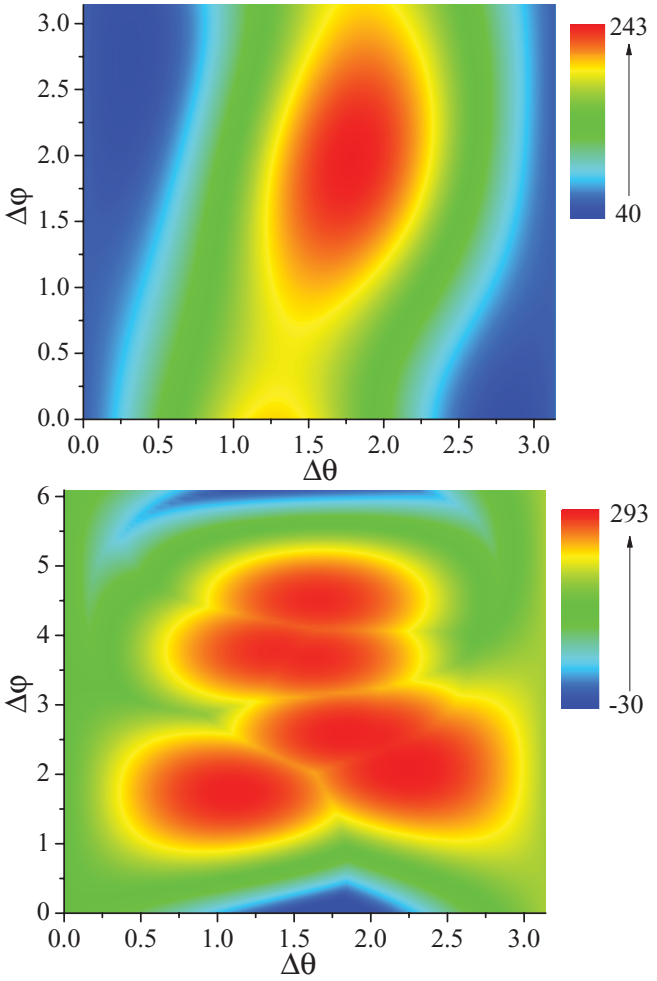

FIG. 12. (Color online) Top: Behavior of Δ [defined in Eq. (8)], in units of cm^{-1} (~0.1 meV) as a function of the angles $\Delta\theta$ and $\Delta\phi$ defining the orientation of the FMO complex, in the case of $\omega_l = -1000$ cm^{-1} and $E_0 = 70$ D^{-1} cm^{-1} $\sim 42 \times 10^7$ V/m. The difference between the maximum and the minimum value is comparable to the thermal energy, and the maximum is obtained for $\Delta\theta \sim 1.75$ and $\Delta\phi \sim 2$, which seems to be the preferred orientation when the sample is subjected to this constant laser field. Bottom: Maximum value of the Rabi frequencies $\vec{\mu}_i \cdot \vec{e}E_0$ vs $\Delta\theta$ and $\Delta\phi$. Notice that the detuning values are much larger than the Rabi frequencies.

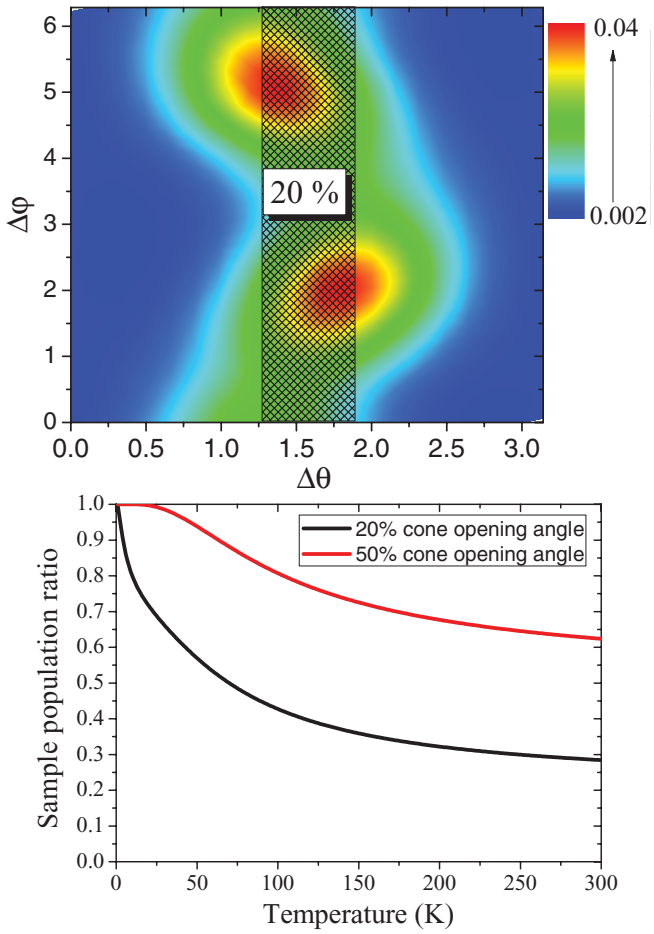

FIG. 13. (Color online) Top: Boltzmann-Gibbs (BG) probability distribution in orienting the FMOs in the sample, as a function of the angles $\Delta\theta$ and $\Delta\phi$, in the case of $\omega_l = -1000$ cm^{-1} and $E_0 = 70$ D^{-1} cm^{-1}. The dashed area represents the region in which we will sum up all of the probabilities in the case, for instance, of a 20% cone opening angle, i.e., 0.2π. Notice, however, that a slightly tilted strip would get a higher probability for the same width and so further improves our results. Bottom: Sample population ratio of FMOs oriented within a cone with some opening angle (20%, i.e., 0.2π, and 50%, i.e., 0.5π), as a function of temperature (K), with $\omega_l = -1000$ cm^{-1}, and $E_0 = 70$ D^{-1} cm^{-1}, according to the BG distribution.

control experiments take of the order of a few picoseconds, which, importantly, is several orders of magnitude shorter than the time for the FMO complexes to lose orientation after the detuned laser beam has been switched off. Hence, we can avoid interference between the orientation laser and the actual optimal control experiment.

X. OPTIMAL PROBE

In the context of controlling a molecular system by optimal femtosecond laser pulses, a similar approach can be reasonably used to optimize the probe pulse absorption in a pump-probe scheme. A successful demonstration of the optimization of the absorbance of the probe pulse by optimal control techniques, but based on a derivative functional equation, was shown for a prototypical molecular three-level system in Ref. [40]. Here we repeat the analysis above for a probe laser pulse applied to the FMO complex by using the CRAB algorithm. In order to compare our theoretical predictions, e.g., in Fig. 7, with the experimental data, since there is no RC in the FMO complex sample used in the laboratory, one has to measure the population in site 3 as a function of time and then calculate the corresponding transfer efficiency. To do that, a probe pulse is applied to the sample and the corresponding absorption intensity is detected. Usually, the probe pulse is Gaussian and on resonance with the site whose population one wants to measure. Here we apply the optimal control tools to analyze whether a shaped pulse can detect the site population, particularly in site 3, with a higher "resolution," as compared to a simpler Gaussian one. Actually, it will turn out that when one considers only a single FMO complex, very high fidelities (99%) are already obtained by a Gaussian pulse oriented along some optimal polarization axis, and the pulse shaping will not give significant improvements. On the other hand, if one has a sample of fully randomly oriented systems, both Gaussian and optimally shaped pulses lead to very low fidelities since the orientation disorder is too strong. However, if a partial orientation would be feasible from the experimental point of view, the control on the pulse shape significantly increases the probability of successfully probing site 3. Specifically, we consider a single FMO complex in the case where, initially, all of the population is in site 3 and we want to find the pulse which is able to detect this population by absorption, i.e., by removing population from the site. Correspondingly, we use $\varepsilon_P = \rho_{33}$ as the error function, where ρ_{33} is the site-3 population. The probe pulse is applied for a time interval of $t = 125$ fs. We find that if there is just one FMO complex in the sample, then the optimization orientates the probe pulse polarization axis along the optimal direction (related to the site-3 dipole moment); however, further optimization of the pulse shape does not bring additional significant gain. Hence a Gaussian pulse will reliably detect the site-3 population (absorption efficiency, i.e., $1 - \varepsilon_P$, of 99%). On the contrary, if this Gaussian pulse, optimally polarized, is applied to a sample of randomly oriented FMOs, then the method does not provide us with a more efficient absorption signal (compared to the traditional way), and is associated to an error of about 50%. If we apply the optimal control algorithm to find the best probe, averaged over 20 isotropic orientations according to the dodecahedron above, this does not improve significantly the results either (data not shown). Finally, we consider the case of a partially oriented sample (10% disorder), particularly within a cone of 0.1π opening angle, and we optimize the pulse along 21 orientations inside this cone, as done above for the pump. Hence, we apply this optimally shaped pulse to a sample of 10^4 FMOs randomly oriented inside this cone, and we compare the absorption efficiency to the case of a Gaussian pulse, polarized along the optimal orientation obtained for a single FMO. We find that the optimally shaped pulse gives a probability of high absorption efficiency (small ε_P), which is more than twice as large as the one with a Gaussian pulse; see Fig. 14. Therefore, in the presence of structural disorder but achieving a partial orientation of the FMOs in the sample, both polarization and shape optimizations may enhance the probe pulse absorption in a pump-probe scheme, which is crucial for an efficient discrimination of dynamical

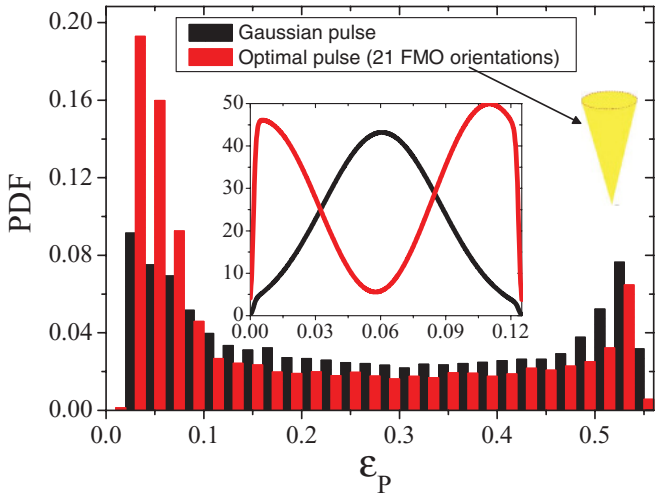

FIG. 14. (Color online) Probability distribution of the quantity ε_P, when the FMO is initially prepared with all the population in site 3 and then subjected a laser probe pulse for a time interval of 125 fs to detect the site-3 population, in the presence of dephasing with rate $\gamma \sim 1$ ps^{-1}. In particular, we consider the case of a Gaussian pulse on resonance with the site 3, i.e., $\omega_l = 0$ cm^{-1}, and polarized along some optimal orientation (with regards to a single FMO), and the case of an optimal pulse obtained by averaging the error function ε_P over 21 directions inside a cone with an opening angle of 0.1π, whose optimal carrier frequency is $\omega_l = 12.63$ cm^{-1}. To get the probability distribution, we apply both pulses to a sample of 10^4 samples randomly oriented inside that cone. Inset: Amplitude (in units of D^{-1} cm^{-1} $\sim 6 \times 10^6$ V/m) of both (Gaussian and optimal) probe pulses.

properties, such as the identification of transport paths discussed here.

XI. CONCLUSION AND OUTLOOK

In summary, the experimental verification of specific quantum features in the dynamics of biomolecular systems in noisy environments [6–12] requires the development of novel experimental tools and theoretical methodology. In this work, we have contributed to this effort with the demonstration that recently developed methods from the theory of optimal control can be combined with ultrafast laser pulses to provide enhanced diagnostic tools, suggesting promising new routes for experiments. In particular, we have introduced and applied the CRAB algorithm for optimal quantum control that was originally developed in quantum information science [19] and used it to determine, for realistic experimental parameters, (weak) pulse shapes that allow for the preparation of arbitrary coherent superpositions with high fidelity. We are also able to reduce the impact of the random orientation of FMO complexes in typical samples and to optimize the readout of the system, maximizing state sensitivity. These methods may serve to provide further experimental confirmation that recent models concerning the interplay of transport processes and environmental noise [6–12] do grasp the main features of the system dynamics. Moreover, optimal control techniques can provide additional tools for the experimental discrimination of Hamiltonian descriptions resulting from different methods [27,34], which would be an important step toward developing more accurate theoretical descriptions of the system-matrix protein environment [24]. In future work, based on the techniques presented here, we are planning to consider more general non-Markovian models [41–43], and other biomolecular complexes, and we will study the importance of multiple excitations in the system. We will also explore the use of CRAB within closed-loop control techniques in this context. These tools will then be experimentally applied to provide optimized setups that, using methods different from multidimensional spectroscopy, allow us to quantitatively probe the functional relevance of quantum coherence, the exploration of which would shed further light on the question as to whether or not quantum correlations are a necessary ingredient for efficient EET in natural conditions.

ACKNOWLEDGMENTS

We acknowledge discussions with Jon Marangos concerning experimental parameters. This work was supported by the EU Integrating projects Q-ESSENCE and AQUTE, the EU STREP project CORNER, SFB/TRR21, the EU Marie-Curie Programme, MIUR-FIRB (Project No. RBFR10M3SB), and the Alexander von Humboldt Foundation.

[1] V. I. Prokhorenko, A. R. Holzwarth, F. R. Nowak, and T. J. Aartsma, J. Phys. Chem. B **106**, 9923 (2002).
[2] G. S. Engel, T. R. Calhoun, E. L. Read, T.-K. Ahn, T. Manal, Y.-C. Cheng, R. E. Blankenship, and G. R. Fleming, Nature (London) **446**, 782 (2007); H. Lee, Y-C. Cheng, and G. R. Fleming, Science **316**, 1462 (2007).
[3] G. Panitchayangkoon, D. Hayes, K. A. Fransted, J. R. Caram, E. Harel, J. Wen, R. E. Blankenship, and G. S. Engel, Proc. Natl. Acad. Sci. USA **107**, 12766 (2010).
[4] E. Collini, C. Y. Wong, K. E. Wilk, P. M. G. Curmi, P. Brumer, and G. D. Scholes, Nature (London) **463**, 644 (2010).
[5] I. P. Mercer, Y. C. El-Taha, N. Kajumba, J. P. Marangos, J. W. G. Tisch, M. Gabrielsen, R. J. Cogdell, E. Springate, and E. Turcu, Phys. Rev. Lett. **102**, 057402 (2009).
[6] M. Mohseni, P. Rebentrost, S. Lloyd, and A. Aspuru-Guzik, J. Chem. Phys. **129**, 174106 (2008).
[7] M. B. Plenio and S. F. Huelga, New J. Phys. **10**, 113019 (2008).
[8] F. Caruso, A. W. Chin, A. Datta, S. F. Huelga, and M. B. Plenio, J. Chem. Phys. **131**, 105106 (2009).
[9] A. Olaya-Castro, C. F. Lee, F. F. Olsen, and N. F. Johnson, Phys. Rev. B **78**, 085115 (2008).
[10] A. W. Chin, A. Datta, F. Caruso, S. F. Huelga, and M. B. Plenio, New J. Phys. **12**, 065002 (2010).
[11] P. Rebentrost, M. Mohseni, I. Kassal, S. Lloyd, and A. Aspuru-Guzik, New J. Phys. **11**, 033003 (2009).
[12] F. Caruso, S. F. Huelga, and M. B. Plenio, Phys. Rev. Lett. **105**, 190501 (2010).

[13] C. Brif, R. Chakrabarti, and H. Rabitz, New J. Phys. **12**, 075008 (2010).
[14] M. Shapiro and P. Brumer, *Principles of the Quantum Control of Molecular Processes* (Wiley, New Jersey, 2003).
[15] J. L. Herek, J. Photochem. Photobiol. A **180**, 225 (2006).
[16] A. P. Peirce, M. A. Dahleh, and H. Rabitz, Phys. Rev. A **37**, 4950 (1988).
[17] J. L. Herek, W. Wohlleben, R. J. Cogdell, D. Zeidler, and M. Motzkus, Nature (London) **417**, 533 (2002); J. Savolainen, R. Fanciulli, N. Dijkhuizen, A. L. Moore, J. Hauer, T. Buckup, M. Motzkus, and J. L. Herek, Proc. Natl. Acad. Sci. USA **105**, 7641 (2008).
[18] B. Brüggemann and V. May, J. Phys. Chem. B **108**, 10529 (2004); Chem. Phys. Lett. **400**, 573 (2004); B. Brüggemann, T. Pullerits, and V. May, J. Photochem. Photobiol. A **180**, 322 (2006); **190**, 372 (2007).
[19] P. Doria, T. Calarco, and S. Montangero, Phys. Rev. Lett. **106**, 190501 (2011).
[20] R. Kosloff, S. A. Rice, P. Gaspard, S. Tersigni, and D. J. Tannor, Chem. Phys. **139**, 201 (1989).
[21] S. A. Rice and M. Zhao, *Optical Control of Molecular Dynamics* (Wiley, New York, 2000).
[22] V. May and O. Kühn, *Charge and Energy Transfer Dynamics in Molecular Systems* (Wiley, Berlin, 2004), Chap. 9.
[23] R. S. Judson and H. Rabitz, Phys. Rev. Lett. **68**, 1500 (1992).
[24] J. Yuen-Zhou, M. Mohseni, J. J. Krich, and A. Aspuru-Guzik, Proc. Natl. Acad. Sci. USA **108**, 17615 (2011).
[25] W. H. Press, S. A. Teukolsky, W. T. Vetterling, and B. P. Flannery, *Numerical Recipes. The Art of Scientific Computing* (Cambridge University Press, New York, 2007).
[26] T. Rowan, Ph.D. thesis, Texas University (Austin), 1990.
[27] J. Adolphs and T. Renger, Biophys. J. **91**, 2778 (2006).
[28] H. Haken and G. Strobl, Z. Phys. **262**, 135 (1973).
[29] H. Lee, Y-C. Cheng, and G. R. Fleming, Science **316**, 1462 (2007).
[30] V. I. Prokhorenko, A. R. Holzwarth, F. R. Nowak, and T. J. Aartsma, J. Phys. Chem. B **106**, 9923 (2002).
[31] D. E. Tronrud, M. F. Smidt, and B. E. Matthews, J. Mol. Biol. **188**, 443 (1986).
[32] S. Montangero, T. Calarco, and R. Fazio, Phys. Rev. Lett. **99**, 170501 (2007).
[33] P. Rebentrost, I. Serban, T. Schulte-Herbrüggen, and F. K. Wilhelm, Phys. Rev. Lett. **102**, 090401 (2009).
[34] D. Hayes and G. S. Engel, Biophys. J. **100**, 2043 (2011).
[35] H. Stapelfeldt and T. Seideman, Rev. Mod. Phys. **75**, 543 (2003).
[36] F. Simoni and O. Francescangeli, J. Phys. Condens. Matter **11**, R439 (1999).
[37] J. J. Chou, S. Gaemers, B. Howder, J. M. Louis, and A. Bax, J. Biomol. NMR **21**, 377 (2001).
[38] D. G. Grier, Nature (London) **424**, 810 (2003).
[39] M. T. W. Milder, B. Brüggemann, v.R. Grondelle, and J. L. Herek, Photosynth. Res. **194**, 257 (2010).
[40] A. Kaiser and V. May, J. Chem. Phys. **121**, 2528 (2004) ; J. Chem. Phys. Lett. **405**, 339 (2005).
[41] J. Prior, A. W. Chin, S. F. Huelga, and M. B. Plenio, Phys. Rev. Lett. **105**, 050404 (2010).
[42] M. Thorwart, J. Eckel, J. H. Reina, P. Nalbach, and S. Weiss, Chem. Phys. Lett. **478**, 234 (2009).
[43] J. Roden, A. Eisfeld, W. Wolff, and W. T. Strunz, Phys. Rev. Lett. **103**, 058301 (2009).